# Sensitive Solution-Processed Bi₂S₃ Nanocrystalline Photodetectors

**Gerasimos Konstantatos, Larissa Levina, Jiang Tang, and Edward H. Sargent***

*Department of Electrical and Computer Engineering, University of Toronto, 10 King's College Road, Toronto, Ontario M5S 3G4, Canada*

## ABSTRACT

Solution-processed nanocrystal optoelectronic devices offer large-area coverage, low cost, and compatibility with a wide range of substrates. Recently, photodetectors and photovoltaics based on spin-coated nanoparticle films have shown tremendous progress in performance. However, high-performance devices reported to date have employed either Pb or Cd, raising concerns regarding environmental impact and regulatory acceptance. Herein we report a high-performance solution-processed photodetector based instead on $Bi_2S_3$ nanocrystals. The devices exhibit photoconductive gain on the order of 10 combined with temporal response on the 10 ms time scale. The resultant solution-processed $Bi_2S_3$ nanorod photoconductive photodetectors are of interest in visible and near-infrared (NIR) wavelength applications requiring video-frame-rate temporal response.

Colloidal nanocrystalline materials have attracted significant interest due to their solution-processibilty. This offers the potential for monolithic low-cost large-scale integration with CMOS electronics. In addition, progress in organic transistors and their integration[1] has led to the development of large-area flexible image sensors.[2−4] Conformal arrays have recently been reported and shown to offer optical advantages compared to planar architectures.[5]

Recently, progress has been reported in light-emitting diodes,[6−8] photodetectors,[9−11] and solar cells[12−14] based on colloidal nanocrystals. These reports, however, share one limiting characteristic: they employ materials containing either metal cations of Pb, Cd, or Hg, or anions of As. The use of these materials could limit widespread adoption in view of environmental and related regulatory concerns.

Recently, colloidal nanocrystals that do not rely on Pb and Cd have seen considerable development: $Ag_2S$,[15] ZnSe:Mg,[16] $Bi_2S_3$,[17] and ZnO[18] have been reported as candidates for optical sensing and light emission. To date, however, only one high-performance device,[19] a photovoltaic, has been reported. This device, based on $Cu_2S$ combined with CdS nanorods, represents a significant step in the direction of heavy-metal-free solution-processed optoelectronics.

Photoconductive photodetectors are sensors for light that, in contrast with photodiodes, are not limited to conveying no more than one electron's worth of current per photon incident; instead, photoconductive photodetectors can exhibit gain. Upon light absorption, an electron−hole pair is generated, and one carrier, the hole for example, is rapidly captured into a long-lived trap. The electron may then flow for a persistence time given by the lifetime of the trap state. The internal photoconductive gain that results is then given by the ratio of the electron lifetime to its transit time across the device. This mechanism boosts the electrical signal from the detector, providing an internal preamplification stage. Low-light detection is thereby facilitated because this gain serves to overcome circuit read-out noise that often limits photodiodes.

The sensitivity of a photodetector must take into account noise in addition to signal. The noise-equivalent power (NEP) describes the lowest incident optical power distinguishable from noise and is equal to the ratio of noise current to responsivity. A more universal figure of merit for photodetecting materials and systems, $D^*$, the specific detectivity, is given in units of Jones and allows comparison among photodetectors having different areas and bandwidths. A high-$D^*$ photodetector has, given its area and detection bandwidth, a desirably low noise-equivalent power.

Photoconductive photodetectors, sensitive in both the short-wavelength infrared[9] and visible[20] wavelengths, have recently been reported based on PbS colloidal quantum dots. These detectors exhibited high photoconductive gain as a result of long carrier lifetime and high mobility. In the present work, we investigate whether it is possible to achieve this desirable mechanism of photoconductive gain in heavy-metal-free materials. We sought materials having a bandgap that would facilitate light detection in the NIR and visible wavelengths. Bismuth sulfide, $Bi_2S_3$, is a direct-bandgap semiconductor with bandgap 1.3 eV and large absorption coefficient,[21] making it an ideal candidate for solution-processed visible-wavelength photodetectors.

* Corresponding author. E-mail: ted.sargent@utoronto.ca.

The photoconductivity of chemically deposited bulk and nanocrystalline $Bi_2S_3$ has been investigated.[22] The complexity of chemical bath deposition renders this process incompatible with monolithic integration of this material onto CMOS platforms. Solution-processed $Bi_2S_3$ nanocrystalline materials have been reported, providing promise for convenient integration. Photoconductivity from solution-processed $Bi_2S_3$ nanocrystals has been reported in the past with responsivity varying from $10^{-5}$,[21] to $10^{-1}$.[17] The time required for the photocurrent to relax to the dark current state was reported to be on the order of several tens of seconds.

Previous reports on the synthesis of $Bi_2S_3$ nanocrystalline materials include chemical deposition techniques,[23] organometallic synthesis based on the reaction of $BiI_3$ with $H_2S$,[17] and the synthesis of colloidal nanorods and nanodots capped with oleylamine.[24] Herein, we report instead an oleic-acid-based organometallic synthesis of $Bi_2S_3$ colloidal nanorods and we optimize and characterize the optoelectronic performance of photodetectors fabricated based on this material. We demonstrate the first solution-processed photodetector based on heavy-metal-free materials to exhibit photoconductive gains on the order of 100, a value that is 3 orders of magnitude higher than previously reported results. The temporal response of devices reported herein is measured on the order of a few tens of ms, representing a 2 order-of-magnitude improvement over previously reported results for $Bi_2S_3$.

We began by seeking a synthetic route that employed oleic acid as the capping ligand. We employed bismuth(III) oleate (bismuth precursor) and hexamethyldisilathiane (HMS, sulfur precursor). The mixture of 1.6 mmol bismuth(III) acetate, 9.8 mmol of oleic acid, and 9.4 mmol of 1-octadecene was heated under vacuum at 90 °C for 16 h. We then introduced an argon atmosphere and heated the flask to 170 °C over the course of 30 min. Then 0.3 mmol of HMS in 2.5 mL of 1-octadecene were injected into the flask and the solution was heated for 2 h at 100 °C. The reaction was then quenched and the temperature of the solution lowered to 30 °C. To isolate the synthesis products, we injected anhydrous methanol and centrifuged. After removing supernatant, the mixture was redispersed in toluene and reprecipitated with methanol. The resultant $Bi_2S_3$ particles were redispersed in toluene.

As seen in the inset of Figure 1a, crystalline nanorods are produced in this synthetic route. The average length of the nanorods is ~22 nm with length distribution of 16%, whereas the average width is ~7 nm with distribution ~34%. The absorption spectrum of the materials, shown in Figure 1a, reveals these $Bi_2S_3$ nanorods to exhibit a bandgap of ~1.3 eV, similar to the published bulk bandgap. The absence of evidence of quantum confinement is consistent with reports of $Bi_2S_3$ nanomaterials of similar size and is explained by the large effective mass of electrons and holes in $Bi_2S_3$, resulting in a relatively small Bohr radius for excitons.[24,25] The large size distribution of the resultant nanocrystals does not have an effect on the absorption spectrum of the solution, for the absorbance is determined by the bulk absorption of $Bi_2S_3$. High-resolution Z-contrast TEM (Figure 1a) reveals the nanorods to be single-crystalline. The XRD diffraction
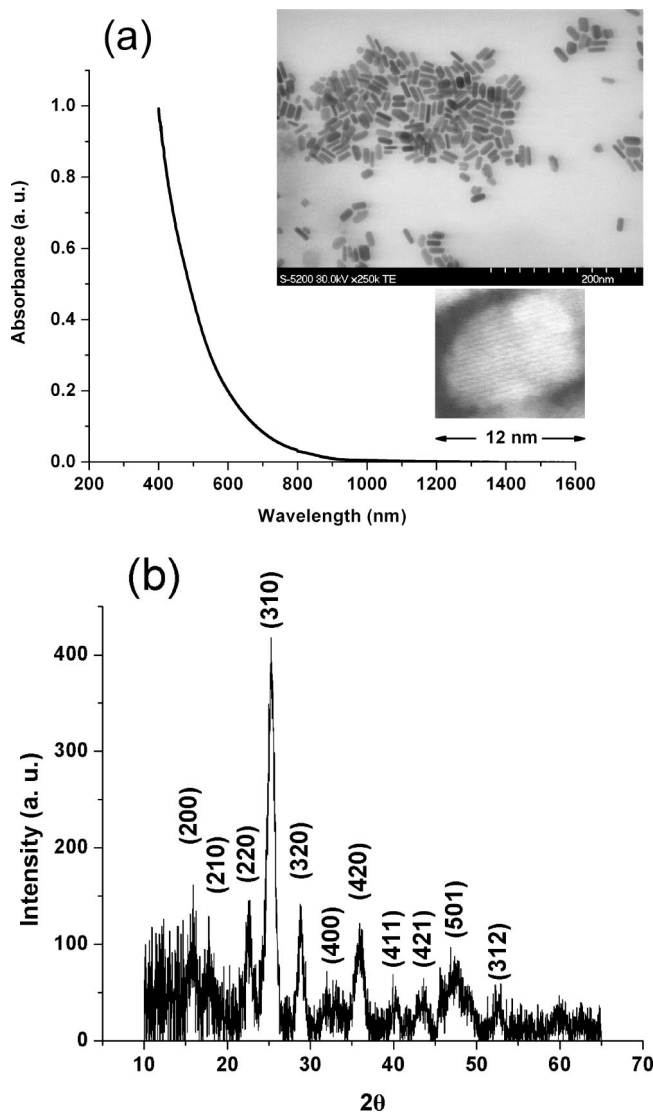


**Figure 1.** (a) Absorbance of $Bi_2S_3$ colloidal nanocrystals. Inset shows a TEM micrograph of the nanocrystals exhibiting a rod-shape structure. $Bi_2S_3$ nanocrystals demonstrate a single-crystalline structure. (b) XRD pattern of $Bi_2S_3$ nanorods.

peaks shown in Figure 1b are in excellent agreement with the orthorhombic structure of $Bi_2S_3$ (JCPDS 02-0391) in peak positions and relative intensities. Oxides such as $Bi_2O_3$ were not detected in XRD spectrum.

The synthesis described above can be modified to produce bismuth sulfide nanodots by reducing the injection temperature to 140 °C and decreasing the growth temperature to 80 °C. However, devices made using dots exhibited a 2 order-of-magnitude lower conductivity and photoconductivity than the nanorod-based devices whose optoelectronic response is discussed herein. We believe the reason for the poor performance of the dot-based devices lies in the poor crystallinity of the material as indicated by XRD results. Poor crystallinity may lead to a high rate of recombination centers and low carrier mobilities.

Photoconductive photodetectors were fabricated by spin-casting $Bi_2S_3$ nanocrystals onto gold interdigitated electrodes on a glass substrate. The interelectrode spacing on the substrate was 5 $\mu$m and their length 3 mm. The thickness of
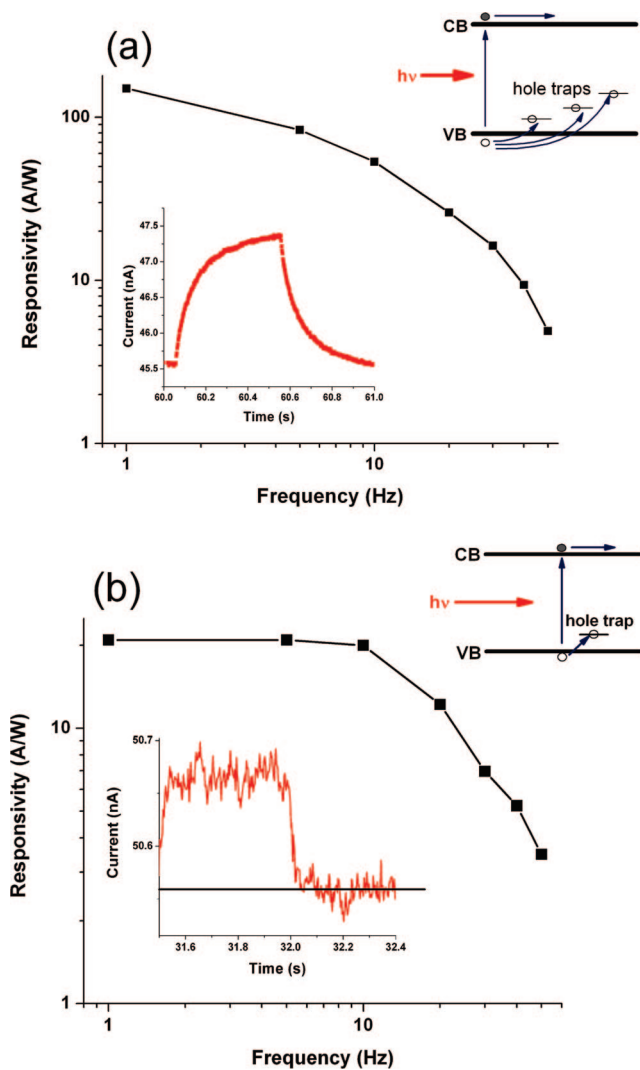
**Figure 2.** Responsivity as a function of modulation frequency for (a) thiol treated devices and (b) thiol treated devices followed by methanol soaking. The detector exhibits a characteristic time constant of $\sim$20 ms. Insets show the temporal response of the detector at optical intensity of $\sim$70 nW/cm.[2] The associated band diagrams are also shown demonstrating the role of the sensitizing centers in each case.

the colloidal quantum dot film was measured to be $\sim$120 nm. The nanoparticles comprising these films were capped with 2 nm long oleate ligands, resulting in very poor conductivity and photoconductivity. A solid-state ligand exchange was thus performed to replace oleic acid with the much shorter and strongly bound ethanethiol: the films were soaked in a $\sim$30% by volume ethanethiol in acetonitrile solution for $\sim$5 min. The resultant films demonstrated conductivity of $1.5 \times 10^{-6}$ S cm$^{-1}$, with dark current density of 12.6 mA/cm$^2$ at 1 V/$\mu$m electric field.[26]

This treatment also led to an orders-of-magnitude increase in photoconductive gain, with treated films showing responsivities in the hundreds of A/W, as shown in Figure 2a. We characterized the dependence of the responsivity of the modulation frequency of the incident optical signal (Figure 2a) and found there was no regime of frequency between 1 and 100 Hz in which the responsivity was constant. This suggested that the processing had generated a number of

different classes of trap states having different lifetimes, ranging from tens of milliseconds to seconds. A plurality of time constants, some unacceptably long, have been observed in previous reports of Bi$_2$S$_3$ photoconductors as well.[22,23] The multiple types of hole traps implicated can be the result of a variety of unpassivated surface states or defect states. It is noteworthy that we achieved similar performance after treating the oleate-capped nanocrystal devices in other short ligands such as acetic acid, formic acid, and benzenethiol: this indicates that the trap states responsible for these long lifetimes pre-existed and could not be passivated by thiol of carboxyl group funtionalities. Similar behavior has been reported in unoptimized PbS quantum dot photoconductive detectors.[27] Multisecond lifetime components prevent such detectors from being used in staring-array video-frame-rate imaging applications. As seen in the time-domain profile of Figure 2a inset, the photocurrent decay persists beyond 1 s, which in imaging results in the appearance of a ghost image.

We therefore sought surface treatments that would passivate long-lived deep trap states, but at the same time preserve the trap states having desirable millisecond lifetimes that provide for a useful photoconductive gain. Trap state engineering based on this principle has been reported in the case of PbS colloidal quantum dot photodetectors.[28] We added an additional solid-state treatment, soaking the devices in methanol for 30 min. Methanol was chosen because alcohols are known to act as chelates[29] on bismuth compounds, forming metal−organic complexes. This treatment resulted in a gain on the order of 10, combined with a much more practically useful temporal response that exhibited a longest time constant of $\sim$23 ms, rendering these devices suited to standard 30 frames-per-second imaging. This is seen in Figure 2b, wherein the responsivity as a function of electrical modulation frequency is flat between 1 and 10 Hz and shows a 3 dB bandwidth of $\sim$20 Hz. The inset of Figure 2b demonstrates the temporal response of the device, exhibiting a complete-relaxation time of the photocurrent back to the dark current level within 100 ms. The accelerated temporal response in these devices is accompanied by a decrease in the photoconductive gain, also to a more practically useful value of order 10. (Photodetector gain is optimally chosen to overcome the electronic noise in read-out circuits, prescribing the need for gains of 5−15; further increases in gain results in overfilling of charge-storage capacitors without further improving sensitivity.) Gain in photoconductors is proportional to the product of carrier lifetime with mobility: in the accelerated devices the carrier lifetime, given by the photocurrent relaxation time, is shorter than the ethanethiol treated devices.

The physical picture of conduction and photoconductivity in our Bi$_2$S$_3$ devices is now discussed. First, with respect to the conduction type, Bi$_2$S$_3$ is reported to be an n-type semiconductor.[22] Consistent with this fact, ohmic contacts have been reported to Bi$_2$S$_3$ using shallow-work-function metals such as aluminum[21] and silver.[23] In our devices, gold contacts have been used, therefore, as seen in Figure 3a, the current−voltage characteristics of the device in dark and illuminated conditions exhibit an onset of linear conduction
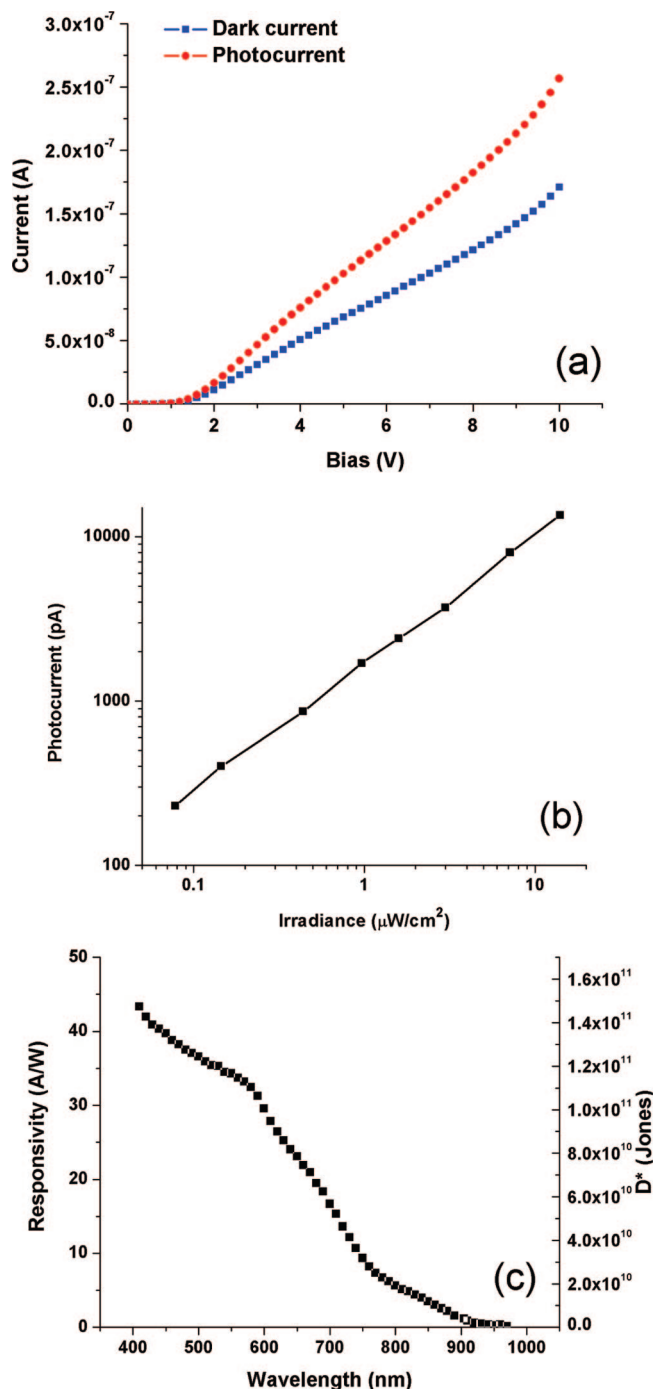
**Figure 3.** Optoelectronic characteristics of the methanol-treated (fast) Bi$_2$S$_3$ photodetector. (a) Current−voltage characteristic of the photoconductive devices under dark and light conditions. (b) Measured photocurrent versus incident optical intensity, the photocurrent exhibits a sublinear dependence on optical power suggestive of sensitized photoconductivity. (c) Spectral responsivity and normalized detectivity at 10 Hz modulation frequency and 1 V/$\mu$m applied electric field.

at an onset bias of ∼1 V. This is consistent with the energy offset of the work function of gold (∼5 eV) relative to the shallow-work-function metals that are known to provide ohmic contact to Bi$_2$S$_3$. Sensitization in these devices stems from hole trap states that capture holes, prolonging the electron carrier lifetime, consistent with other reports on Bi$_2$S$_3$ photodetectors.[17,23] The current−voltage characteristics

are supportive of this mechanism: Below 1 V, there is no photoconductive gain observed due to the noninjecting character of the contacts. Beyond 1 V, the gold electrodes can become injecting contacts for electrons as shown by the significant dark conductance in this bias regime. It is only then that photoconductive gain can also be observed because electron injection is required for carrier replenishment.

The dependence of photocurrent on incident optical power, shown in Figure 3b, exhibits a power dependence of ∼0.77, i.e., $I_p \sim P^{0.77}$, suggestive of a sensitized photoconductor having an exponential distribution of trap states.[30] This is unlike the case of nonsensitized Bi$_2$S$_3$ photoconductors reported in the literature[23] in which a linear dependence of photocurrent on optical power accompanies the lack of photoconductive gain.

The spectral responsivity of the Bi$_2$S$_3$ photodetector,[31] shown in Figure 3c, demonstrates the efficient coverage of the visible wavelengths by this material for light sensing applications. We measured the noise current of the detector,[32] enabling us to determine the normalized detectivity $D^*$ as function of wavelength in Figure 3c. The noise current was ∼2.9 pA/Hz$^{1/2}$ resulting in $D^*$ on the order of 10$^{11}$ Jones across the visible.

In sum, we report herein the first solution-processed photoconductive detector to be made using heavy-metal-free materials. The device provides substantial photoconductive gain in the tens to hundreds of charge carriers collected per incident photon, and temporal response on the order of tens of milliseconds, rendering it suited to video frame rate imaging. This performance was achieved through the development of a novel synthetic procedure that led to Bi$_2$S$_3$ single-crystalline nanorods capped with oleate ligands, followed by development of methods that decrease inter-nanoparticle spacing using shorter capping molecules and further combined with trap state engineering necessary to achieve the combination of multi-10-fold photoconductive gain and millisecond temporal response. In addition to the promising performance of this material for sensing applications, this work reports on the electronic properties of this material employing the phenomenon of photoconductivity as a probe for the investigation of carrier transport and trapping processes.

**References**
(1) Crone, B.; Dodabalapur, A.; Lin, Y.-Y.; Filas, R. W.; Bao, Z.; LaDuca, A.; Sarpeshkar, R.; Katz, H. E.; Li, W. *Nature* **2000**, *403*, 521–523.
(2) Yu, G.; Wang, J.; McElvain, J.; Heeger, A. *Adv. Mater.* **1998**, *10*, 1431–1434.
(3) Nausieda, I.; Ryu, K.; Kymissis, I.; Akinwande, A. I.; Bulović, V.; Sodini, C. G. *IEEE Trans. Electron Devices* **2008**, *55*, 527–532.
(4) Someya, T.; Kato, Y.; Iba, S.; Noguchi, Y.; Sekitani, T.; Kawaguchi, H.; Sakurai, T. *IEEE Trans. Electron Devices* **2005**, *52*, 2502–2511.
(5) Cho Ko, H.; Stoykovich, M. P.; Song, J.; Malyarchuk, V.; Choi, W. M.; Yu, C. J.; Geddes, J. B., III.; Xiao, J.; Wang, S.; Huang, Y.; Rogers, J. A. *Nature* **2008**, *454*, 748–753.
(6) Coe, S.; Woo, W. K.; Bawendi, M.; Bulovic, V. *Nature* **2002**, *420*, 800–803.
(7) Konstantatos, G.; Huang, C.; Levina, L.; Lu, Z.; Sargent, E. H. *Adv. Funct. Mater.* **2005**, *15*, 1865–1869.

(8) Tessler, N.; Medvedev, V.; Kazes, M.; Kan, S.; Banin, U. *Science* **2002**, *295*, 1506–1509.

(9) Konstantatos, G.; Howard, I.; Fischer, A.; Hoogland, S.; Clifford, J.; Klem, E.; Levina, L.; Sargent, E. H. *Nature* **2006**, *442*, 180–183.

(10) Oertel, D. C.; Bawendi, M. G.; Arango, A. C.; Bulovic, V. *Appl. Phys. Lett.* **2005**, *87*, 213505–213507.

(11) Boberl, M.; Kovalenko, M. V.; Gamerith, S.; List, E. J. W.; Heiss, W. *Adv. Mater.* **2007**, *19*, 3574–3578.

(12) Gur, I.; Fromer, N. A.; Geier, M. L.; Alivisatos, A. P. *Science* **2005**, *310*, 462–465.

(13) Klem, E. J. D.; MacNeil, D. D.; Cyr, P. W.; Levina, L.; Sargent, E. H. *Appl. Phys. Lett.* **2007**, *90*, 183113–183115.

(14) Koleitat, G.; Levina, L.; Shukla, H.; Myrskog, S.; Hinds, S.; Pattantyus-Abraham, A. G.; Sargent, E. H. *ACS Nano* **2008**, *2*, 833–840.

(15) Wang, D.; Hao, C.; Zheng, W.; Peng, Q.; Wang, T.; Liao, Z.; Yu, D.; Li, Y. *Adv. Mater.* **2008**, *9999*, 1–5.

(16) Thakar, R.; Chen, Y.; Snee, P. T. *Nano Lett.* **2007**, *7*, 3429–3432.

(17) Suarez, R.; Nair, P. K.; Kamat, P. V. *Langmuir* **1998**, *14*, 3236–3241.

(18) Jin, Y.; Wang, J.; Sun, B.; Blakesley, J. C.; Greenham, N. C. *Nano Lett.* **2008**, *8*, 1649–1653.

(19) Wu, Y.; Wadia, C.; Ma, W.; Sadtler, B.; Alivisatos, A. P. *Nano Lett.* **2008**, *8*, 2551–2555.

(20) Konstantatos, G.; Clifford, J.; Levina, L.; Sargent, E. H. *Nat. Photonics* **2007**, *1*, 531–534.

(21) Cademartiri, L.; Malakooti, R.; O'Brien, P. G.; Migliori, A.; Petrov, S.; Kherani, N.; Ozin, G. A. *Angew. Chem., Int. Ed.* **2008**, *47*, 3814–3817.

(22) Nair, M. T. S.; Nair, P. K. *Semicond. Sci. Technol.* **1990**, *5*, 1225–1230.

(23) Popova, B.; Tanusevski, A.; Grodzanov, I. *J. Solid State Chem.* **2005**, *178*, 1786–1798.

(24) Malakooti, R.; Cademartiri, L.; Akcakir, Y.; Petrov, S.; Migliori, A.; Ozin, G. A. *Adv. Mater.* **2006**, *18*, 2189–2194.

(25) Riley, D. J.; Waggett, J. P.; Wijayantha, K. G. U. *J. Mater. Chem.* **2004**, *14*, 704–708.

(26) Current−voltage characteristic as well as transient dark and photo-conductivity were measured using a 4155 Agilent semiconductor parameter analyzer .

(27) Konstantatos, G.; Sargent, E. H. *Appl. Phys. Lett.* **2007**, *91*, 173505–173508.

(28) Konstantatos, G.; Levina, L.; Fischer, A.; Sargent, E. H. *Nano Lett.* **2008**, *8*, 1446–1450.

(29) Domenico, P.; Salo, R. J.; Novick, S. G.; Schoch, P. E.; Van Horn, K.; Cunha, B. A. *Antimicrob. Agents Chemother.* **1997**, *41*, 1697–1703.

(30) Rose, A. *Concepts in Photoconductivity and Allied Problems*; Robert E. Krieger Publishing: New York, 1972.

(31) For spectral responsivity measurements, a bias was applied to the sample connected in series with a 2 MΩ load resistor. Illumination was provided by a white light source (ScienceTech Inc. TH-2) dispersed by a Triax 320 monochromator and mechanically chopped at the frequency of interest. Optical filters were used to prevent grating overtones from illuminating the sample. The voltage across the load resistor was measured using a Stanford Research Systems SR830 lock-in amplifier. The intensity transmitted through the monochromator at each wavelength was precalibrated, and controlled via a variable attenuator, to be ∼500 nW/cm2. Photocurrent was then extracted by the ratio of the recorded voltage in the lock-in amplifier over the load resistor.

(32) Dark current noise in the photodetectors was measured using a Stanford Research SR830 lock-in amplifier. The devices were biased using alkaline batteries and testing in an electrically shielded and optically sealed probe station on a floating table to minimize vibrational noise. The reported noise current, normalized to the measurement bandwidth, divided by the responsivity under the same measurement conditions, yielded the noise equivalent power (NEP). The normalized detectivity $D*$ was obtained as a function of wavelength, applied bias, and center frequency by dividing the square root of the optically active area of the device by the NEP.

NL802600Z